ACS central science

http://pubs.acs.org/journal/acscii

Research Article

Intersubunit Coupling Enables Fast CO_2-Fixation by Reductive Carboxylases

Hasan DeMirci,*[,] Yashas Rao, Gabriele M. Stoffel, Bastian Vögeli, Kristina Schell, Aharon Gomez, Alexander Batyuk, Cornelius Gati, Raymond G. Sierra, Mark S. Hunter, E. Han Dao, Halil I. Ciftci, Brandon Hayes, Fredric Poitevin, Po-Nan Li, Manat Kaur, Kensuke Tono, David Adrian Saez, Samuel Deutsch, Yasuo Yoshikuni, Helmut Grubmüller, Tobias J. Erb,* Esteban Vöhringer-Martinez,* and Soichi Wakatsuki*

Cite This: *ACS Cent. Sci.* 2022, 8, 1091−1101

Read Online

ACCESS | Metrics & More | Article Recommendations | Supporting Information

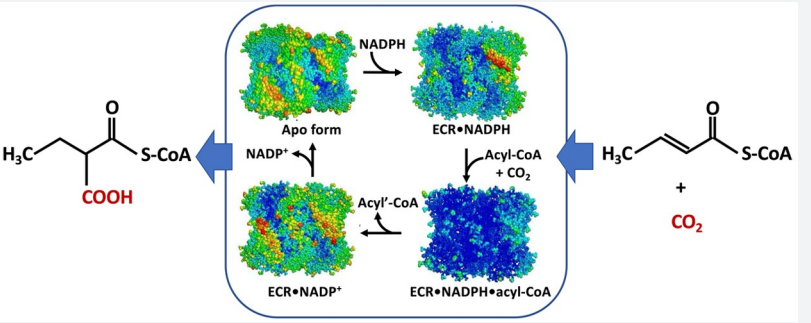

ABSTRACT: Enoyl-CoA carboxylases/reductases (ECRs) are some of the most efficient CO_2-fixing enzymes described to date. However, the molecular mechanisms underlying the extraordinary catalytic activity of ECRs on the level of the protein assembly remain elusive. Here we used a combination of ambient-temperature X-ray free electron laser (XFEL) and cryogenic synchrotron experiments to study the structural organization of the ECR from *Kitasatospora setae*. The *K. setae* ECR is a homotetramer that differentiates into a pair of dimers of open- and closed-form subunits in the catalytically active state. Using molecular dynamics simulations and structure-based mutagenesis, we show that catalysis is synchronized in the *K. setae* ECR across the pair of dimers. This conformational coupling of catalytic domains is conferred by individual amino acids to achieve high CO_2-fixation rates. Our results provide unprecedented insights into the dynamic organization and synchronized inter- and intrasubunit communications of this remarkably efficient CO_2-fixing enzyme during catalysis.

INTRODUCTION

The capture and conversion of atmospheric CO_2 remains a challenging task for chemistry, resulting in an ever-increasing interest to understand and exploit CO_2 fixation mechanisms offered by biology. Nature has evolved different enzymes capable of capturing and/or converting CO_2, including biotin-dependent CoA carboxylases, which incorporate CO_2 into different alkyl-CoA esters, formate dehydrogenases, which directly reduce CO_2 into the single-carbon compound formate, and RubisCO, the central enzyme in the Calvin−Benson−Bassham cycle of photosynthesis that produces two molecules of 3-phosphoglycerate from ribulose-1,5-bisphosphate and CO_2.[1−4] The recently discovered family of enoyl-CoA carboxylases/reductases (ECRs) encompasses some of the most efficient CO_2-fixing enzymes found in nature to date.[1] With respect to the catalytic rate, for instance, ECR family members from primary metabolism outcompete RubisCO by more than 1 order of magnitude, which makes them exquisite models to study the molecular basis of efficient CO_2 catalysis.[2,5]

ECRs catalyze the reduction of various α,β-unsaturated enoyl-CoAs into the corresponding alkylmalonyl-CoA esters using the reduced form of the cofactor nicotinamide adenine dinucleotide phosphate (NADPH). Hydride transfer from NADPH to the substrate generates a reactive enolate species, which acts as a nucleophile that attacks a bound CO_2 molecule (Figure 1a).[2,5−7] However, the structural details of the carboxylation reaction have remained elusive, in part due to the lack of high-resolution

Received: January 19, 2022
Published: April 25, 2022

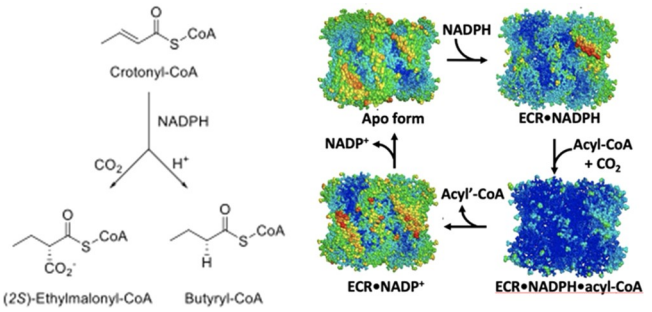

Figure 1. Reaction scheme and structural organization of the *K. setae* ECR complex. (a) Carboxylation reaction scheme of ECR. (b) Anisotropic B-factors of the tetramer of the different ECR complexes solved in this study are shown color coded according to the B factors (blue for low values and red for high values).

structures of ECRs containing catalytic intermediates and carboxylated products.

Until recently, five structures of ECRs have been reported. These ECRs all have different substrate specificities, ranging from short (PDB: 3HZZ, 3KRT)- to long-chain (4A0S[8]) and aromatic enoyl-CoA substrates (4Y0K[9]), and are from different biological backgrounds, including primary (i.e., central carbon) metabolism (PDB: 4GI2) and secondary metabolism (PDB: 4A0S, 4Y0K). However, most of them cocrystallized with only NADPH or $NADP^+$ and do not contain CO_2, enoyl-CoA substrates, or acyl-CoA products.

In a recent study, we reported the ternary structure of the ECR (EC 1.3.1.85) from *K. setae* in a complex with ethylmalonyl-CoA and NADPH (PDB: 6OWE) and identified four active site residues critical to binding and accommodation of CO_2 at the monomer level.[10] Yet, the molecular mechanism of the extraordinary rate enhancement of CO_2 fixation by ECR tetramers remains enigmatic. This is even more notable, as ECR complexes from primary metabolism, such as the *K. setae* ECR, show on average almost 30-fold higher CO_2 fixation rates in comparison to those ECR complexes from secondary metabolism, despite having very high structural similarities. Overall, this work indicated that ECRs from primary metabolism must use specific mechanisms that allow them to enhance CO_2 fixation dramatically in comparison to their structurally closely related homologues from secondary metabolism.

Here, we aimed at providing a mechanistic understanding of the fast carboxylation reaction of the *K. setae* ECR on the level of the overall oligomeric complex. We first determined four high-resolution *K. setae* ECR structures in different conformational states: the apo form and three holo forms in a binary complex with the reduced cofactor NADPH, in a ternary complex with NADPH and butyryl-CoA, and a binary complex with the oxidized cofactor $NADP^+$ (Figure 1b).

Our high-resolution structures show that the tetrameric complex assumes a pair of dimers geometry. In this complex, the central oligomerization domains of the *K. setae* ECR remain essentially unchanged, while the peripheral catalytic domains move significantly to provide two sets of active site conformations—open and closed forms—upon binding of the NADPH cofactors in the presence of substrates. This coordinated motion is enabled by a tight coupling of catalytic domains across the pairs of dimers, which we could trace to the role of individual amino acids far away from the active site. Using computer simulations and kinetic experiments, we provide compelling evidence that synchronization across the pair of dimers through "swing and twist motions" is crucial for the *K. setae* ECR to achieve high catalytic rates. We further demonstrate that subunit communication within a dimer is essential to synchronize open and closed states. Altogether, our results unveil a dynamic intersubunit synchronization of the *K. setae* ECR complex that is essential for the functional organization of one of nature's most efficient CO_2-fixing enzymes during catalysis.

RESULTS AND DISCUSSION

Apo ECR Is a Symmetric Homotetramer, Readily Accessible for Cofactor and Substrate Binding. We first determined the apo form of the ECR crystal structure from *K. setae* at 1.8 Å resolution using synchrotron X-ray crystallography at cryogenic temperature (Table S1 in the Supporting Information). The asymmetric unit contains one homotetramer composed of four subunits arranged in a pair of dimers geometry similar to those of previously reported binary and ternary ECR complexes, crotonyl-CoA carboxylase/reductase AntE in complex with $NADP^+$ (PDB: 4Y0K) and 2-octenoyl-CoA

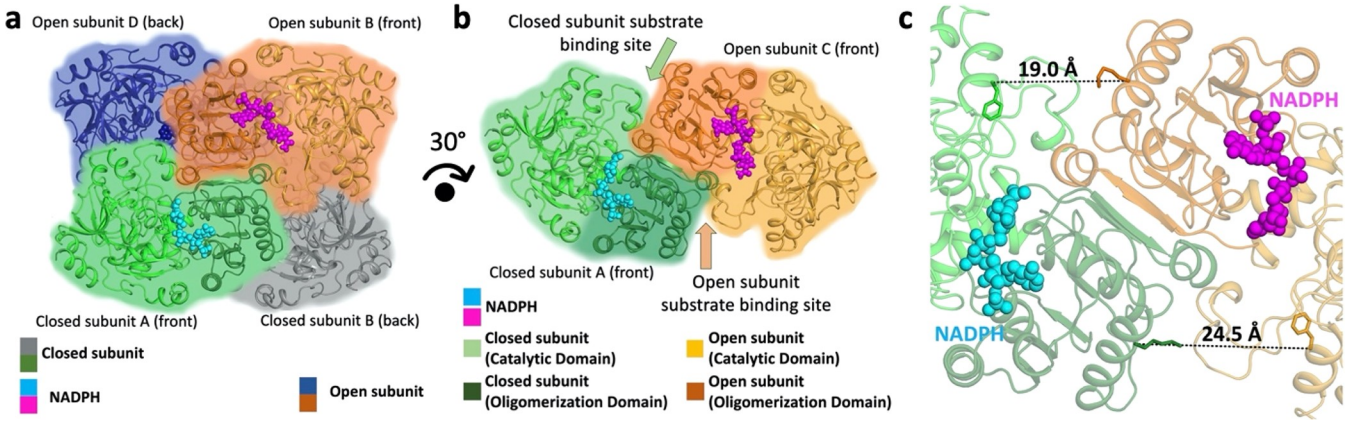

Figure 2. Binding of NADPH results in global and local conformational changes in *K. setae* ECR. (a) NADPH-bound tetramer complex that is organized as pair of dimers, a pair of closed (green) and open (orange) subunits, and another pair containing closed (gray) and open (blue) subunits. (b) The foreground dimer with open (orange)- and closed-form (green) subunits rotated by 30° from the view in (a). Each subunit is composed of a catalytic and an oligomerization domain. (c) Comparison of the putative substrate binding sites between the open- and closed-form subunits.

https://doi.org/10.1021/acscentsci.2c00057
ACS Cent. Sci. 2022, 8, 1091−1101

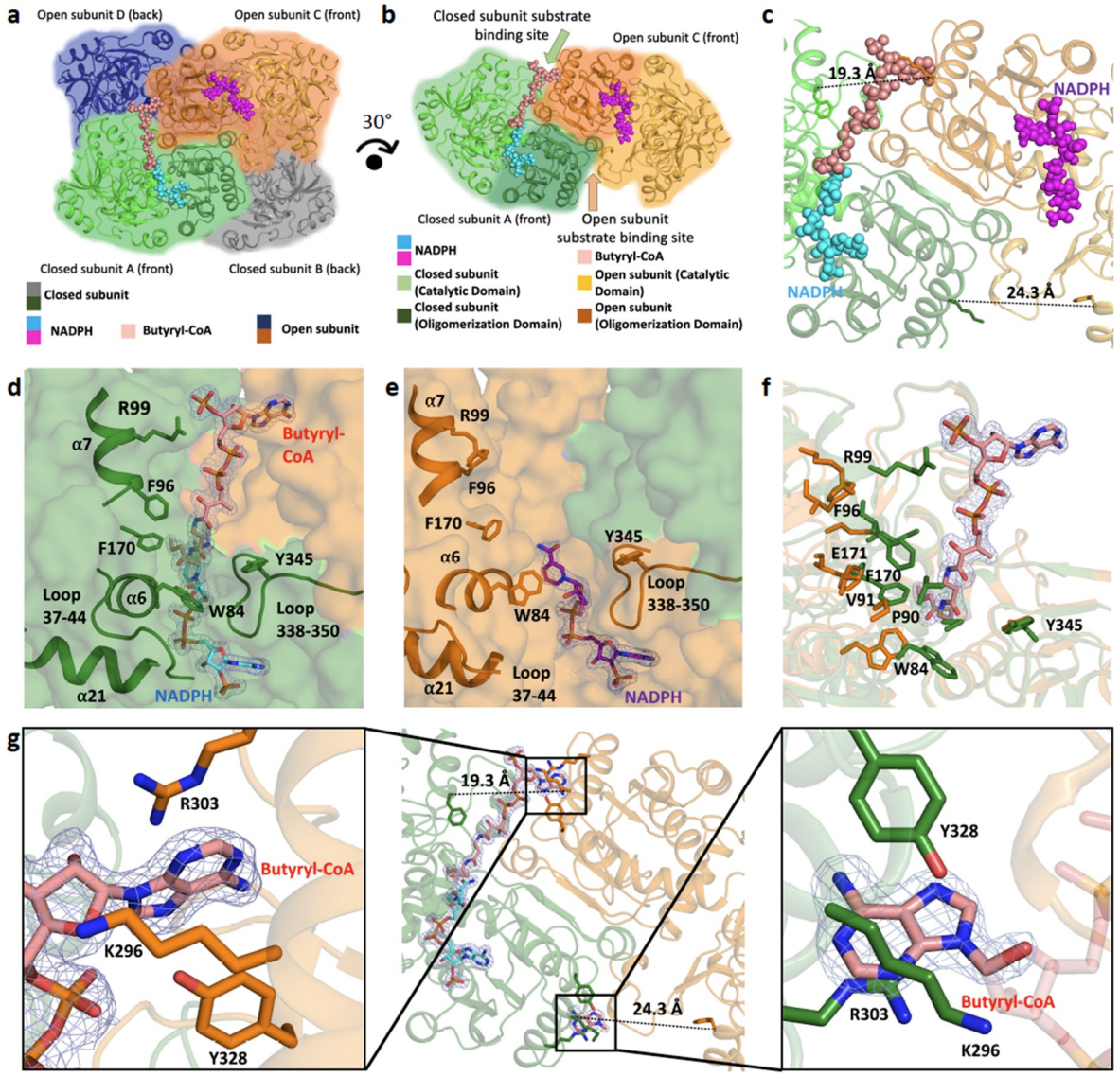

Figure 3. Structure of the ternary ECR complex. (a) ECR tetramer in a complex with NADPH and butyryl-CoA organized as a pair of dimers, the foreground dimer with one closed subunit (green) with NADPH and butyryl-CoA, an open (orange) subunit containing NADPH, and another pair in the background with one closed (gray) and one open (blue) subunit. (b) The foreground dimer with closed (green) and open (orange) subunits, rotated by 30° from the view in (a). Butyryl-CoA and NADPH atoms are represented as spheres. (c) Comparison of the product binding sites between the open- and closed-form subunits. (d) Cartoon and stick representation of the closed-form subunit active site. In (d–g), simple $2F_o - F_c$ density contoured at the 1.5 σ level is shown for butyryl-CoA, or pa ortion thereof, and NADPH within 3 Å from the molecules. (e) Cartoon and stick representation of the open-form subunit active site. (f) Superposition of the open-form subunit onto the closed-form subunit with a stick representation of the residues surrounding butyryl-CoA. (g) Butyryl-CoA binding in both open- and closed-form subunits with the electron density of the bound butyryl-CoA and NADPH at the active site of the closed subunit (green) and the adenine ring of butyryl-CoA at the active site of the open subunit (only the adenine ring electron density is visible). Left inset: the adenine binding pocket of the open-form subunit stabilizing the adenine ring of butyryl-CoA that stretches into the adjacent closed-form subunit. Right inset: the adenine binding pocket of the closed-form subunit holding the adenine ring of butyryl-CoA. Note that only the adenine ring of butyryl-CoA has visible electron density, while the rest of the molecule is disordered, and hence is indicated by a transparent stick model. In both cases, three residues of the adjacent subunits, K296, R303, and Y328, together hold the adenine ring.

carboxylase/reductase CinF in complex with $NADP^+$ and 2-octenoyl-CoA, (PDB: 4A0S), respectively. Overall, the *K. setae* ECR tetramer shows a noncrystallographic, close to D_2 (dihedral) symmetry with four conformationally identical subunits (Figures S1 and S2). The tetrameric oligomer state of the ECR apo enzyme is further supported by size-exclusion chromatography, which showed that the 51.2 kDa protein eluted as a single peak at 205 kDa (Figure S3).

Each ECR subunit consists of two domains—a larger catalytic domain formed by residues 1–212 and 364–445, and a smaller oligomerization domain formed by residues 212–363 (Figure S4A). The oligomerization domain comprises a Rossmann fold[11] with repeating $\alpha\beta$-motifs that form a 6-stranded β-sheet (β12–β17). The 6-stranded β-sheets of two neighboring subunits are combined into one 12-stranded β-sheet, forming the core of one dimer, subunits A/C and B/D. Two of these Rossmann fold domains form the tetrameric complex's core (Figure S4B). The catalytic domains of the *K. setae* ECR are located at the periphery of the tetrameric complex. The active site cavities in the apo form are open and accessible for both

https://doi.org/10.1021/acscentsci.2c00057
ACS Cent. Sci. 2022, 8, 1091–1101

cofactors and substrates. We also determined the structure of $NADP^+$-bound ECR at cryogenic temperature and found that it is rather similar to that of the apo form structure, although $NADP^+$ molecules are bound in all four subunits. We postulate that the same crystallization conditions used for both structures might have resulted in the same space group ($P2_12_12_1$) with similar crystal contacts, which might have kept the $NADP^+$ bound ECR tetramer in the apo form. The $NADP^+$-bound subunits are less rigid in comparison, and some residues show greater variations (Figures S1 and S2).

Cofactor Binding Breaks Tetramer Symmetry and Induces Formation of a Pair of Dimers. In order to understand the effects of binding of NADPH, a cofactor before reaction as opposed to the spent cofactor $NADP^+$ described above, we then determined the *K. setae* ECR-NADPH binary complex's crystal structure at 2.4 Å resolution using serial femtosecond X-ray crystallography (SFX) at ambient temperature (Figure 2 and Table S1).[12−15] In all four subunits, NADPH binds with its adenine moiety in the oligomerization domain and spans the catalytic domain, where its nicotinamide moiety is located (Figure S5).

Notably, NADPH binding breaks the dihedral D_2 symmetry observed in the apo-form tetramer, while symmetry about the *y* axis is retained, resulting in a noncrystallographic, almost cyclic C_2 symmetry (Figure S1). In the NADPH*ECR binary complex, each of the two dimers, A/C and B/D, loses its 2-fold symmetry, giving rise to closed (A and B) and open (C and D) subunits (Figure 2a,b and Figure S1). In the A and B subunits, the cofactor binding pocket is compressed inward, which seals the NADPH cofactor within the catalytic domain, resulting in a "closed-form" state (Figure 2b). On the other hand, the C and D subunits show open cofactor-binding pockets, referred to hereafter as an "open-form" state. The substrate-binding pocket in the open-form C or D subunit is more than 5 Å wider than the closed A or B subunit (Figure 2c). When they were taken together, these structures indicated that during catalysis the enzyme differentiates into a pair of dimers (A/C and B/D dimers, respectively), with one closed (A or B) and one open subunit (C or D) per dimer.

Cofactor−Substrate Complex Indicates Half-Site Reactivity within Each Dimer. We next investigated the effects of substrate binding to the *K. setae* ECR tetramer complex and determined its ternary complex structure with the substrate analogue butyryl-CoA and NADPH at 1.7 Å resolution (Figure 3). The structure is overall very similar to the conformation of the ECR*NADPH binary complex with the noncrystallographic, pseudo-C_2 cyclic symmetry (Figure 3a and Figure S1). It comprises two sets of open- and closed-form subunits that overlay very well with those of the ECR*NADPH binary complex (Figures S1 and S2). The NADPH cofactor appears to be bound to all active sites; however, only the closed-form subunits A and B also contain electron density for the complete butyryl-CoA thioester, while the open-form subunits (C and D) show only the adenine group electron density of the butyryl-CoA thioester (Figure 3a,b). The presence of the intact butyryl-CoA thioester in the active site of the closed-form subunits strongly suggests that the A and B conformations represent the Michaelis complex in which the substrate and cofactor are positioned for catalysis. In contrast, the open-form subunits (C and D) represent catalytically incompetent ternary complexes.

The binding of the cofactor and substrates in the closed-form ECR subunit is achieved by loops 37−44, 88−94, 338−350 and helices 6, 7, and 21 of the catalytic domains, which creates multiple interactions of the protein with the NADPH and butyryl-CoA (Figure 3d−f). Notably, the CoA-thioester extends from the closed-form active site out to the oligomerization domain of the neighboring open-form subunit in the same dimer pair (from A to C in the A/C dimer, or from B to D in the B/D dimer), where R352 and Y353 from the open-form subunit (C or D) interact with the phosphate backbone of the CoA. The adenosine tail of the CoA extending from the closed-form subunit interacts with the three residues Y328, K296, and R303 that form an adenine binding pocket at the neighboring open-form subunit (Figure 3g). When we inspected CoA-thioester binding in the open-form subunits, we also observed the electron density in the adenine binding pocket of the neighboring closed form subunits (A or B), strongly indicating that the CoA-thioester was bound (Figure 3g, right inset). However, the electron density beyond the adenine ring becomes invisible, suggesting that the part of the CoA molecule reaching into the open-form subunit's active site remains flexible and disordered, which is corroborated by the higher B-factors of the catalytic domain (Figure 1, bottom right).

To evaluate the substrate's flexibility in the open- and closed-form subunits, quantum mechanical/molecular mechanics (QM/MM) simulations on a dimer of subunits A and C that account for the electronic degrees of freedom of the substrate were combined with MM simulations of the pair of dimers (tetramer) with substrates initially modeled in the open and bound closed subunits to reach longer time scales. These simulations showed that the substrate in the closed subunit had significantly lower temperature factors (B-factors) in comparison to that in the open subunit (Figures S6−S8 and Movies S1a−e and S2a−e). In the open subunit, the acyl moiety shows a high degree of flexibility in the active site, in agreement with the higher B-factors observed in crystal structures.

Together, crystallographic structures and QM/MM simulations indicate that upon substrate binding the enzyme complex splits into two catalytically competent (A or B) and incompetent subunits (C or D) per dimer, suggesting that the enzyme tetramer operates with half-site reactivity, in which catalytically competent and incompetent active sites alternate during catalysis.[16−19]

Swing and Twist Motions of Peripheral Catalytic Domains Are Coupled within and across a Pair of Dimers to Promote Catalysis. To study the switching between the open and closed forms of the ternary complex, we used computer simulations. Starting from the ternary crystal structure with NADPH and butyryl-CoA, we modeled the natural substrate crotonyl-CoA to carry out all-atom molecular dynamics simulations of the catalytic active enzyme (see Supplementary Methods). In our simulations, the closed subunit remained closed and maintained crotonyl-CoA in the active site when the dynamics of the substrate were restrained to maintain specific protein−substrate/cofactor interactions. However, in simulations without substrate restraints, the acyl moiety of the substrate left the active site, resulting in a conformational change of the closed subunit to the open form.

To study this conformational change in detail, we eliminated the crotonyl-CoA substrate from the ternary complex, creating an ECR*NADPH binary complex with two closed and two open subunits. In all 10 100 ns simulations of the tetramers, the closed subunits underwent a fast conformational change during the first tens of nanoseconds (the same was observed when we started from the X-ray binary ECR*NADPH structure). To further describe this conformational change, we used principal

https://doi.org/10.1021/acscentsci.2c00057
ACS Cent. Sci. 2022, 8, 1091−1101

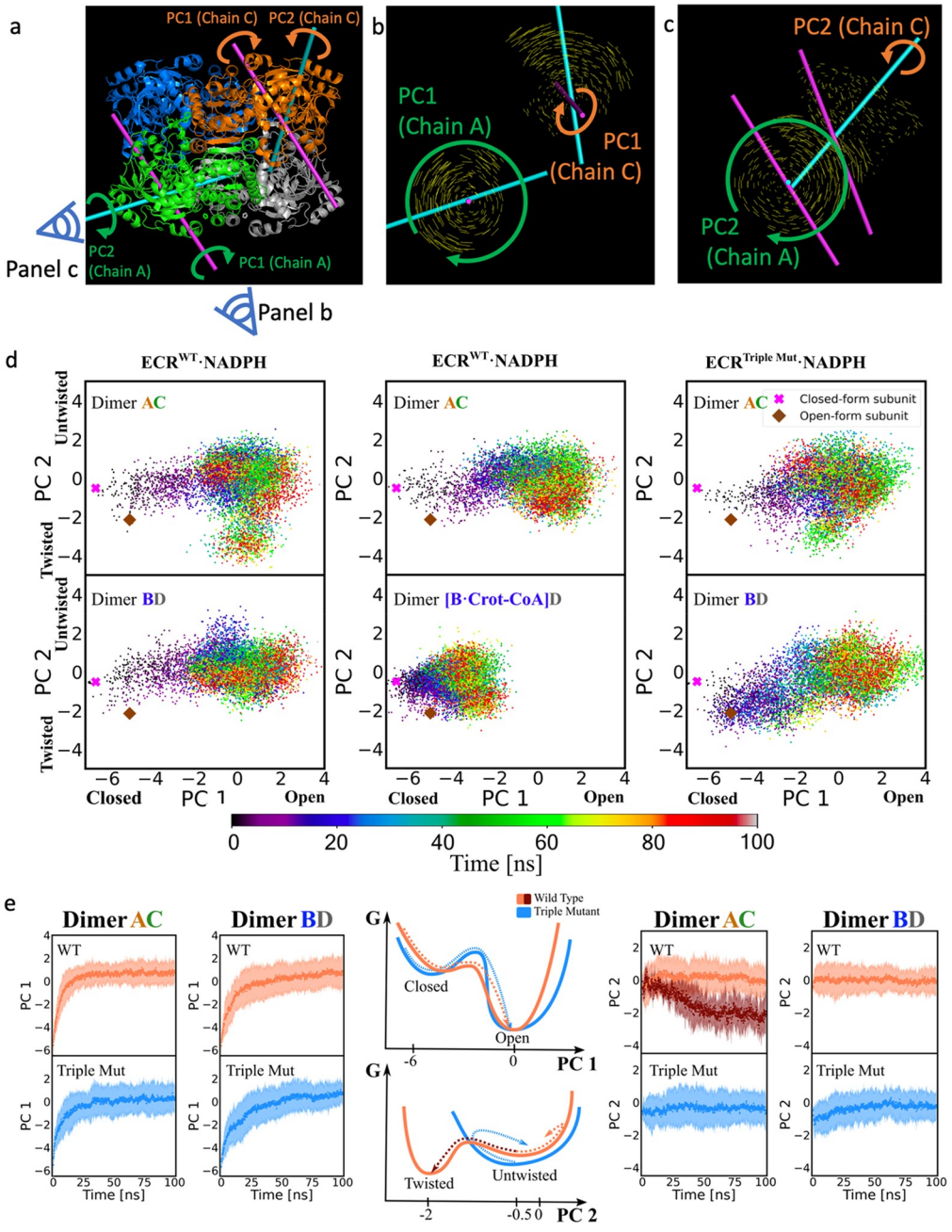

Figure 4. Molecular dynamics simulations and principal component analyses reveal that the absence of the substrate induces a transition between the open and closed forms of the catalytic domain in the ECR tetramer and a twist in the subunits, which would move a bound substrate toward the NADPH cofactor. (a) Representation of the swing motion of the catalytic domain in dimer AC described by the first principal component (PC1) and the twist motion of one subunit to the other by PC2. This twist motion would bring a bound substrate closer to the NADPH cofactor. PC1 and PC2 axes of A (closed) and C (open) subunits are superimposed on the ternary tetramer structure in the same orientation as in Figure 3a, showing the functional relevance of PC1 as opening−closing and PC2 as twisting of the catalytic domains. (b, c) Sets of vectors between initial and final Cα positions of the catalytic domains are shown viewed along the PC1 (b) and PC2 (c) axes of subunit A as shown on the bottom left of (a). (d) Projection of 10 100 ns trajectories on the first two principal components of the wild type binary system with the NADPH cofactor ECR^{wt}·NADPH (crosses and diamonds represent the open- and closed-form subunits from the X-ray structure, respectively). The middle panels show the projection on the same PCs for the ECR^{wt} ternary complex bearing only one substrate in the B subunit of the BD dimer ([B·Crot-CoA]D). The right panels represent the dynamics of the E151D/N157E/N218E triple variant with the NADPH cofactor (ECR$^{Triple.Mut}$·NADPH) on the same eigenvectors. Colors of each points represent the time frame according to the scale bar at the bottom. (e) Mean values and 1.5 times the standard deviation of the principal components of 10 trajectories as a function of simulation time for each dimer in the WT (orange) and E151D/N157E/N218E triple variant (blue) ECR·NADPH complex. Time traces of PC1 are shown on the left and those of PC2 on the right. In the middle, free energy profiles as a function of PC1 and PC2 were derived for the wild type (orange) and variant (blue) on the basis of the observed kinetics. The triple variant with slower opening kinetics (PC1) is consistent with a barrier in the transition to the open form, and its larger standard deviation suggests a shallower minimum in the closed form. The free energy profile of PC2 corresponds to a broad minimum for the triple variant because of the larger standard deviation observed in the kinetics and a large barrier to reach the twisted conformation observed in the WT dynamics (brown trajectory shown in dimer AC for PC2 on the right).

https://doi.org/10.1021/acscentsci.2c00057
ACS Cent. Sci. 2022, 8, 1091−1101

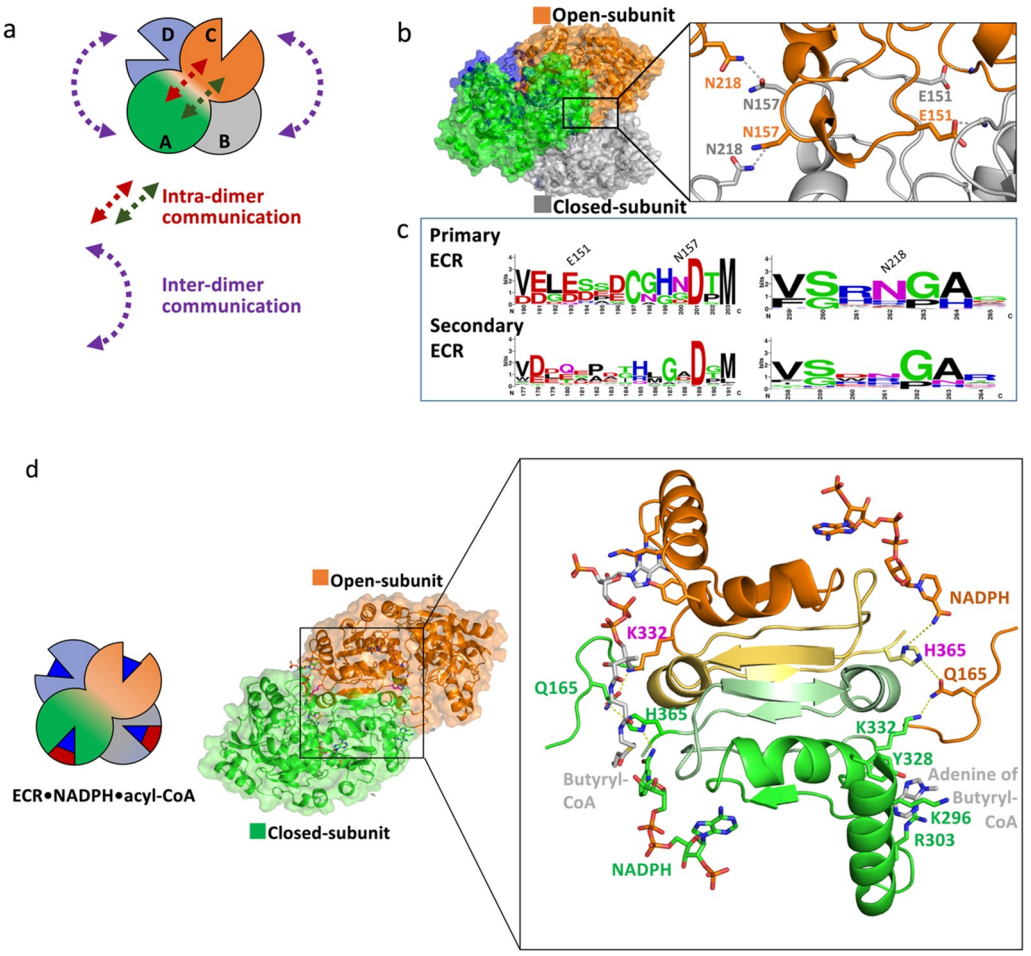

Figure 5. Inter- and intradimer communications drive fast CO_2 fixation by *K. setae* ECR. (a) Two distinct sets of communications: interdimer interactions between the catalytic domains from two dimers (purple arrows) and intradimer communication between the open and closed subunits within each dimer (brown arrows). (b) Interdimer catalytic domain interface and positions of selected amino acids that were mutated in this study to affect the interface between the two catalytic domains (open-form subunit in orange and closed form subunit in gray). The right panel shows the mutual H-bonding interaction between N218 and N157 from open- and closed-form subunits and H-bonding between E151 and the N atom from the protein backbone. (c) Alignment of ECR protein sequences from the primary (upper row) and the secondary (lower row) metabolisms represented as sequence logos. The numbering of residues, above the first row, is according to their position in the *K. setae* ECR. (d) Communication between the closed (green) and open (orange) subunits across the two dimers of the *K. setae* ECR. In the closed conformation the contacts between NADPH-H365-E165 and K332 of the adjacent open subunit allow for the correct intradimer communication. In the open conformation the communication network is compromised, as indicated by the increased distances between the amino acid side chains that cause the incorrect positioning of the nicotinamide ring of NADPH.

component analysis (PCA) of the backbone Cα atom's positions of 10 combined 100 ns trajectories of both dimers. The 100 ns time scale was enough to describe the primary steps of the conformational changes, as evidenced by the convergence analysis (Figures S9 and S10). The first principal component (PC1) represents a transition of the closed to the open form, and the second principal component (PC2) describes a twist motion of one subunit to the other subunit in each dimer. In both cases the catalytic domains move relative to the oligomerization domains (Figure 4a−c and Movies S3 and S4). The rotation axes of PC1 and PC2 cross with each other with close to 90° inside the catalytic domain in each subunit. The two PC1 axes of subunits A and C are nearly parallel, corresponding to the closed-open motions, while the PC2 axes show the twisting motions of the catalytic domains (Figure 4b,c).

To characterize the dynamics, we compared the projections of all 10 dimer trajectories on PC1 and PC2. Dimer A/C opens its closed subunit first, associated with PC1, followed by a twist motion characterized by PC2 in some of the simulations (Figure 4d and Figure S10). This twist motion rotates the catalytic domain of the empty, now open form active site in subunit A, which would push a bound crotonyl-CoA substrate toward the NADPH cofactor in the C subunit. The B/D dimer's dynamics, on the other hand, were mainly governed by the closed subunit opening represented by PC1, likely because of the initial structural differences of the two dimers.

After characterizing the conformational transitions associated with the presence or absence of CoA substrate, we asked whether the dynamics of one dimer in the tetramer complex is coupled to that of the other dimer. Computer simulations allowed us to address this question by studying the dynamics of a hypothetical system that lacks the substrate in only one active site. Removing crotonyl-CoA from subunit A, we expected the—now empty—"closed" active site subunit to transition to the open form, inducing the twist motion in the A/C dimer observed before, and the other closed subunit B still bearing the substrate remains closed, if the two dynamics of the pair of dimers are uncoupled. The projection of 10 100 ns trajectories

https://doi.org/10.1021/acscentsci.2c00057
ACS Cent. Sci. 2022, 8, 1091−1101

Table 1. Steady -State Analysis of *K. setae* ECR and Variants Targeting the Catalytic Domain Interface between the Pair of Dimers[a]

	crotonyl-CoA			NADPH		CO_2	
enzyme	K_M (μM)	K_i (μM)	k_{cat} (s^{-1})	K_M (μM)	k_{cat} (s^{-1})	K_M (μM)	k_{cat} (s^{-1})
wild type	21 ± 2	3650 ± 810	103 ± 3	37 ± 4	86 ± 2	90 ± 10	78 ± 2
E151D	28 ± 2	1960 ± 250	20 ± 1	72 ± 11	17 ± 1	80 ± 10	21 ± 1
N157E	515 ± 75		22 ± 1	105 ± 27	17.1 ± 0.4	40 ± 6	14 ± 0
N218E	272 ± 37		3.7 ± 0.2	66 ± 9	3.3 ± 0.0.2	840 ± 150	3.3 ± 0.2
E151D/N157E/N218E	245 ± 25		1.1 ± 0.0	26 ± 3	0.7 ± 0.0	440 ± 40	0.9 ± 0.0

[a]Michaelis−Menten curves of *K. setae* ECR and its variants are provided in Figure S14.

on PC1 and PC2 confirmed that the empty active site (A in the A/C dimer) undergoes a conformational change to the open form (Figure 4d), whereas the dimer containing the substrate (B in the B/D dimer) remained in a closed conformation (see Figure S11 for a comparison to the simulation with two substrates maintaining the closed state). Importantly, however, none of the A/C dimer trajectories showed a significant change in PC2 associated with the twist motion observed in the binary ECR*NADPH complex, indicating that the twist motion is only initiated once the other dimer B/D adopts the open conformation.

In summary, our molecular dynamics simulations indicate that the absence or release of the substrate triggers a conformational transition from the closed to the open conformation and that coupled dynamics of the two dimer pairs induce an additional twist motion after opening the closed subunit of the other dimer pair.

Three Remote Amino Acids Couple Catalysis between Pairs of Dimers. Given the coordinated motions of the catalytic domains during catalysis, how is catalysis synchronized across the enzyme complex (i.e., across dimers A/C and B/D)? One intriguing aspect of the ECR tetramer structures is that the catalytic domains share a common interface of 1636 $Å^2$ between the pairs of dimers (Figure 5a,b), suggesting that they move together as rigid bodies.

What are the molecular determinants that synchronize catalysis across the pair of open/closed form dimers? The intercatalytic domain interface is predominantly hydrophobic with some electrostatic interactions (Figure 5b). Most notable are N218, which forms a hydrogen bond to N157 of the adjacent subunit of the other dimer, and E151 interacting with the backbone nitrogen atom of N133 (and/or A134) of the neighboring subunit of the other dimer (Figure 5b). A multiple sequence alignment using CLUSTAL W[20] showed that E151, N218, and N157 are highly conserved in ECRs from primary (i.e., central carbon) metabolism with faster CO_2-fixation kinetics (average k_{cat} 28 s^{-1}), but not in ECRs from secondary metabolism with an average k_{cat} of 1.2 s^{-1} (Figure 5c), which raised the question about their potential role in promoting catalysis in primary metabolic ECRs.

Notably, mutation of these residues that are more than 20 Å away from the active site dramatically affected the kinetic parameters of *K. setae* ECR (Table 1). In the E151D variant, the k_{cat} value decreased by a factor of 5, demonstrating that weakening the interaction between catalytic domains has profound effects on the enzyme's catalytic rate. Mutations that targeted the asparagine interaction network also showed substantial effects on the catalytic rate and affected the K_M value of substrate binding. Most notable were a N218E single variant and E151D/N157E/N218E triple variants that decreased the k_{cat} values by more than 25- and 100-fold, respectively, highlighting that communication through the interface of the catalytic domains of the pair of dimers is an essential determinant of the catalytic rate in *K. setae* ECR.

To confirm that the oligomerization state of the different complexes was not altered through these mutations, we used gel filtration and native gel analysis (Figure S3). Gel filtration under the same conditions as for our kinetic measurements showed that all enzyme variants remained tetramers, while a native gel analysis conducted under more disruptive conditions showed slight increases in the dimer and monomer fractions. Overall, our mutational and kinetic data supported the hypothesis that synchronization of catalytic domains contributes to the catalytic rate and is conferred through the hydrogen-bond network at the pair of dimers interfaces.

To study the effect of the E151D/N157E/N218E mutations on the synchronization of catalytic domains and the conformational transitions of the binary NADPH*ECR complex, we used computer simulations as discussed above. The projection of 10 100 ns trajectories on the previously defined eigenvectors displayed the same opening transition of both dimers in the initially closed binary NADPH*ECR triple variant complex (Figure 4d). We analyzed the time traces of their first two principal components (mean ± 1 std) of both dimers in the tetramer to spot the differences between the WT enzyme and the triple variant (see Figure 4e). Notably, the triple variant opens the closed form more slowly than the WT enzyme and presents a broader distribution of values in both dimers during transition. The observed kinetics are consistent with a free energy profile along PC1, according to which the variant must cross a higher free energy barrier to reach the open form (scheme in Figure 4e). The broader distribution during the transition is caused by a shallower energy minimum of the closed form of the triple variant. For PC2, the dynamics for the WT and the triple variant also differ. The triple variant presents a broader distribution associated with a shallow free energy minimum and shifted minima, causing the two systems to evolve in opposing directions at the beginning of the simulation. Interestingly, only the WT can pass the free energy barrier to a twisted state in some of the trajectories (shown in brown in Figure 4e). Overall, these results confirm that the E151D/N157E/N218E mutation at the dimer interfaces changes the free energy landscape of conformational transitions considerably. The communication between the dimers is reduced, as the triple variant does not share the WT's concerted dynamics that are characterized first by an opening motion and then a twist of one subunit to the other. This twist motion of the open subunit will push the bound substrate to the NADPH cofactor and might be directly coupled to the first step of the ECR reaction: i.e., the hydride transfer.

In summary, computer simulations and kinetic data of the triple variant indicate that coupling the dynamics of the two dimers is conferred by three conserved amino acids in ECRs

https://doi.org/10.1021/acscentsci.2c00057
ACS Cent. Sci. 2022, 8, 1091−1101

Table 2. Apparent Michaelis–Menten Parameters of *K. setae* ECR and Variants Targeting the Adenine Binding Pocket as Mean Values ± Standard Error[a]

	crotonyl-CoA			crotonyl-pantetheine	
enzyme	K_M (μM)	K_i (μM)	k_{cat} (s^{-1})	K_M (μM)	k_{cat} (s^{-1})
wild type	21 ± 2	3650 ± 810	103 ± 3	8660 ± 530	37 ± 1
K296A	107 ± 11		68 ± 2		
Y328F	11 ± 2	4671 ± 1693	80 ± 3		
K296A/Y328F	190 ± 30		39 ± 2		
K296A/R303A/Y328F	2180 ± 280		29 ± 2	7770 ± 110	42 ± 3
K296A/R303 K/Y328F	830 ± 140		53 ± 2		
Q165A	27 ± 4		56 ± 3	5630 ± 520	8.6 ± 0.3
K332A	450 ± 130		38 ± 7	2980 ± 510	0.3 ± 0.0

[a]Michaelis–Menten curves of *K. setae* ECR and its variants are provided in Figure S14.

from primary metabolism (E151, N157, and N218) and is essential to reach fast CO_2 fixation kinetics in comparison to their counterparts from secondary metabolism that lack those residues.

CoA Binding Synchronizes Open and Closed Subunits within a Dimer. In addition to an interdimer domain interaction, the two subunits in each dimer bind different parts of the substrate in the open and closed forms through the adenine binding pocket and the active site (intradimer interaction, Figure 5a). We hypothesized that this shared substrate binding between neighboring subunits could also contribute to the mechanism of fast, synchronized catalysis.

To understand the role of substrate adenine binding in catalysis, we characterized the kinetics of different single, double, and triple variants of the adenine binding site (Figure 3g and Table 2). Mutations in the adenine binding pocket, particularly of R303, strongly increased the apparent K_M value of the CoA substrate as expected and decreased the enzyme's apparent k_{cat} value by a factor of 2–3. Notably, when we used crotonyl-pantetheine, a truncated substrate lacking the adenosine moiety, a comparable decrease in k_{cat} value was also observed for the WT enzyme, suggesting that substrate interactions at the adenine binding pocket indeed contribute to catalysis. However, when we compared the kinetics of the WT enzyme with a truncated substrate to that of triple variant K296A/R303A/Y328F, in which adenosine binding was completely disturbed, the two variants behaved almost identically, strongly supporting the argument that binding of the adenine residue of the CoA substrate in the WT is important for high catalytic activity.

We noticed that the substrate's adenine binding pocket is directly followed by a loop, which carries a lysine residue (K332) that interacts with the neighboring subunit's active site. K332 from the open-form subunit engages in a hydrogen-bonding network with the nicotinamide of the NADPH cofactor bound to the closed-form subunit through Q165 and H365 of the neighboring subunit (Figure 5d). These interactions are not observed in the active site of the open-form subunit (Figure 5d), raising the question of whether the hydrogen-bonding network connected to the adenine binding pocket might be necessary for catalysis.

In variants K332A and Q165A, k_{cat} was decreased by 2–3-fold, and for K332A, an additional increase in the apparent K_M for crotonyl-CoA was observed, indicating some effect of these residues on the catalytic rate (as well as substrate binding in case of K332) (Table 2). When we tested these variants again with the truncated substrate analogue crotonyl-pantetheine, the catalytic activity in the Q165A variant was reduced by 4-fold, while that of the K332A variant was reduced by more than 2 orders of magnitude in comparison to the WT with a truncated substrate. More notably, the K_M had not changed much between the WT and the two different variants (where it has even slightly improved), strongly suggesting that Q165 and K332 are not involved in substrate accommodation but rather synchronization of catalysis between open and closed subunits within the dimer. In conclusion, adenine binding and the loop carrying the residues K332 and Q165 are necessary to synchronize catalysis between the two subunits within the dimer to drive fast CO_2 fixation in the *K. setae* ECR, providing the molecular basis of how catalysis might be synchronized between the open- and closed-form subunits within one dimer.

Half-Site Reactivity with Almost Fullly Occupied Active Sites Drives Fast CO_2 Fixation. Our structural studies of the *K. setae* ECR revealed unprecedented details on the functional organization of one of nature's most efficient and fastest CO_2-fixing enzymes. During catalysis, the enzyme complex differentiates into distinct functional subunits. The binding of the NADPH cofactor and substrates forces the homotetrameric apo enzyme into a pair of dimers. Each dimer is constituted of open- and closed-form subunits. In the closed-form subunits, the NADPH cofactor and CoA substrate are aligned with each other, suggesting that this is the catalytically competent state. The open-form subunits bind the cofactor and the substrate adenine rings, but the rest of the acyl-CoA substrate remains flexible and invisible in the active site. Thus, the open-subunit active sites represent a catalytically incompetent state that is preorganized for a subsequent round of catalysis. Overall, this structural reorganization of the ECR complex strongly supports the idea that the enzyme operates with "half-site reactivity".[16−18] Catalysis is synchronized across the enzyme tetramer and alternates between the open- and closed-form subunits to increase the overall catalytic efficiency of the complex.

It is worth noting that half-site reactivity does not assume (or require) half-site occupancy. Indeed, all four subunits of the *K. setae* ECR tetramer ternary complex contain both NADPH and substrates (products). However, in the open-form subunits, only electron density for the adenine groups of the CoA thioester is observed (Figure 3g). The "half-site reactivity" is also consistent with a negative, rather than positive, cooperativity, as almost all our kinetics data indicate.

To understand if the conventional half-site reactivity theory can be applied to the ECR tetramer case, we created a model for the enzyme kinetics assuming positive or negative cooperativity between the pairs of dimers. Instead of treating the four subunits as independent entities, we hypothesized that the two pairs of ECR dimers would cycle through the CO_2-fixing reactions in

https://doi.org/10.1021/acscentsci.2c00057
ACS Cent. Sci. 2022, 8, 1091−1101

synchrony: i.e., when one dimer switches from the open−close to the closed−open states, the other dimer would do the opposite, closed−open to open−closed states. Using this model, we simulated the case with just one dimer with two subunits working in negative or positive cooperativity using the method described by Hill and Levitski[21] (Figure S12). For a thorough investigation of how cooperativity, positive or negative, enhances the overall reaction rate of the *K. setae* ECR, we incorporated all the parameters in Hill and Levitski's model in our simulation. It turned out that only negative cooperativity could explain our experimental observations that ECR activity in the WT tetramer is increased by 2 orders of magnitude in comparison to the triple variant E151D/N157E/N218E, in which synchronization is decoupled (Table 1). Our simulations yielded a 90% probability that both active sites are occupied with substrates/products and NADPH/$NADP^+$ (p22), while only 10% are half-occupied (p12 + p21) (Figure S12). Almost none of the dimers are empty (p11), which agrees with the occupancy of our experimentally determined structures of the ternary complex.

To synchronize half-site reactivity, the interaction of the catalytic domains across and within the pairs of dimers is crucial. When the latter is perturbed in the *K. setae* ECR (e.g., through triple mutant E151D/N157E/N218E or by disturbance of the adenosine binding pocket), the catalytic rate of the enzyme is severely diminished. This observation is consistent with other theoretical and experimental data on half-site reactivity. The synchronization of distant catalytic subunits has been calculated to enhance the catalytic rate of enzymes by up to 20-fold.[21,22] Mutation of a single amino acid that couples the two catalytic sites of heptose isomerase GmhA reduced the catalytic rate to 6% of wild-type activity.[23] Perturbing the interaction network in *Escherichia coli* thymidylate synthase, another example of an enzyme with half-site reactivity,[24] caused a 400-fold decrease in k_{cat},[25,26] demonstrating that domain interactions are essential in promoting enzyme catalysis.[27]

While our structural, biochemical, and simulation data indicate that the *K. setae* ECR achieves high catalytic rates by synchronizing active sites, this might not necessarily be true for other ECRs. A differentiation into a pair of dimers was not observed in NADPH-bound or ternary structures of other ECRs (e.g., PDB 4Y0K and 4A0S, respectively, which share substantial amino acid identity) (Figure S13). Note, however, that ECRs fall into two different classes: primary ECRs (such as the *K. setae* ECR) that operate in central carbon metabolism and secondary ECRs (such as 4Y0K) that provide extender units for synthesizing polyketides in secondary metabolism. Whereas primary ECRs are under intense evolutionary pressure and show on average k_{cat} values of 28 s^{-1},[28] secondary ECRs are not selected for high catalytic rates, which is also reflected by a 1 order of magnitude smaller average k_{cat} value (k_{cat} = 1.2 s^{-1}).[28] Thus, it might be tempting to speculate that secondary ECRs are not selected for high turnover rates during catalysis and, therefore, might not exhibit synchronized half-site reactivity, which is further supported by the observation that the residues E151, N218, and N157, conferring synchronization at the complex interface, are not conserved in secondary ECRs (Figure 5c).

CONCLUSIONS

Altogether, our work revealed the structural-dynamics determinants explaining the substantial rate enhancement achieved by enoyl-CoA carboxylase/reductase through coordinated catalytic domain motions in comparison to unsynchronized catalytic reactions (e.g., in the four monomers of the triple variant E151D/N157E/N218E). The X-ray structures of the apo-form, binary and ternary ECR complexes provide the end states of these coordinated catalytic domain motions. A PCA analysis of extensive molecular dynamics simulations delineates an atomistic picture of the coupled motions, with one opening and closing motion of the active site and a twist motion that might aid the substrate binding and product release. A further analysis shows that negative cooperativity and half-site reactivity are the governing principles of the substantial enhancement of the overall reaction rate. Active site synchronization can be traced down to individual amino acids at the complex interface and the adenine binding pocket of the CoA substrate. These residues associated with the coupling of the catalytic domains across the different dimers are conserved among highly efficient ECRs from primary metabolism, enhancing the overall catalytic rates by more than a factor of 30 in comparison to their counterparts in secondary metabolism.

METHODS

No unexpected or unusually high safety hazards were encountered. Details of experimental and computational methods are described in Supplementary Methods. Briefly, these contain methods of the amplification and cloning of the *K. setae* ECR, site-directed mutagenesis of its residues at the subunit interface, adenine binding residues and intradimer communication residues, as well as cell lysis, protein purification, characterization of the oligomeric state of the enzyme, and spectrophotometric enzyme assays. The chemical synthesis of CoA-esters and an analysis of ethylmalonyl-CoA stability are also described. Finally, we include detailed methods on the crystallization of *K. setae* ECR complexes, data collection, processing, and structure determination, QM/MM simulations of NADPH and substrate in the open and closed subunits of the ECR dimer, and molecular dynamics simulations of the conformational changes in the ECR tetramer.

ASSOCIATED CONTENT

Supporting Information

The Supporting Information is available free of charge at https://pubs.acs.org/doi/10.1021/acscentsci.2c00057.

Additional figures, discussions, methods and a table as desribed in the text (PDF)
Movie as described in the text (MOV)
Movie as described in the text (MOV)
Movie as described in the text (MOV)
Movie as described in the text (MOV)
Movie as described in the text (MOV)
Movie as described in the text (MOV)
Movie as described in the text (MOV)
Movie as described in the text (MOV)
Movie as described in the text (MOV)
Movie as described in the text (MOV)
Movie as described in the text (MOV)
Movie as described in the text (MOV)
Transparent Peer Review report available (PDF)

AUTHOR INFORMATION

Corresponding Authors

Hasan DeMirci − *Biosciences Division, SLAC National Accelerator Laboratory, Menlo Park, California 94025, United*

https://doi.org/10.1021/acscentsci.2c00057
ACS Cent. Sci. 2022, 8, 1091−1101

States; PULSE Institute, SLAC National Accelerator Laboratory, Menlo Park, California 94025, United States; Department of Molecular Biology and Genetics, Koc University, 34450 Sariyer/Istanbul, Turkey; Email: hdemirci@ku.edu.tr

Tobias J. Erb − *Department of Biochemistry and Synthetic Metabolism, Max Planck Institute for Terrestrial Microbiology, D-35043 Marburg, Germany; LOEWE Center for Synthetic Microbiology (SYNMIKRO), 35032 Marburg, Germany;* orcid.org/0000-0003-3685-0894; Email: toerb@mpi-marburg.mpg.de

Esteban Vöhringer-Martinez − *Departamento de Físico Química, Facultad de Ciencias Químicas, Universidad de Concepción, Concepción 4030000, Chile;* orcid.org/0000-0003-1785-4558; Email: evohringer@udec.cl

Soichi Wakatsuki − *Biosciences Division, SLAC National Accelerator Laboratory, Menlo Park, California 94025, United States; Structural Biology Department, Stanford University, Stanford, California 94305, United States;* orcid.org/0000-0001-5896-7968; Email: soichi.wakatsuki@stanford.edu

Authors

Yashas Rao − *Biosciences Division, SLAC National Accelerator Laboratory, Menlo Park, California 94025, United States; Departamento de Físico Química, Facultad de Ciencias Químicas, Universidad de Concepción, Concepción 4030000, Chile*

Gabriele M. Stoffel − *Department of Biochemistry and Synthetic Metabolism, Max Planck Institute for Terrestrial Microbiology, D-35043 Marburg, Germany*

Bastian Vögeli − *Department of Biochemistry and Synthetic Metabolism, Max Planck Institute for Terrestrial Microbiology, D-35043 Marburg, Germany*

Kristina Schell − *Department of Biochemistry and Synthetic Metabolism, Max Planck Institute for Terrestrial Microbiology, D-35043 Marburg, Germany*

Aharon Gomez − *Departamento de Físico Química, Facultad de Ciencias Químicas, Universidad de Concepción, Concepción 4030000, Chile;* orcid.org/0000-0003-4820-4697

Alexander Batyuk − *Linac Coherent Light Source, SLAC National Accelerator Laboratory, Menlo Park, California 94025, United States;* orcid.org/0000-0002-9393-2880

Cornelius Gati − *Biosciences Division, SLAC National Accelerator Laboratory, Menlo Park, California 94025, United States; Structural Biology Department, Stanford University, Stanford, California 94305, United States*

Raymond G. Sierra − *Linac Coherent Light Source, SLAC National Accelerator Laboratory, Menlo Park, California 94025, United States*

Mark S. Hunter − *Linac Coherent Light Source, SLAC National Accelerator Laboratory, Menlo Park, California 94025, United States*

E. Han Dao − *Biosciences Division, SLAC National Accelerator Laboratory, Menlo Park, California 94025, United States; PULSE Institute, SLAC National Accelerator Laboratory, Menlo Park, California 94025, United States*

Halil I. Ciftci − *PULSE Institute, SLAC National Accelerator Laboratory, Menlo Park, California 94025, United States*

Brandon Hayes − *Linac Coherent Light Source, SLAC National Accelerator Laboratory, Menlo Park, California 94025, United States*

Fredric Poitevin − *Linac Coherent Light Source, SLAC National Accelerator Laboratory, Menlo Park, California 94025, United States*

Po-Nan Li − *Biosciences Division, SLAC National Accelerator Laboratory, Menlo Park, California 94025, United States; Electrical Engineering Department, Stanford University, Stanford, California 94305, United States;* orcid.org/0000-0002-7917-7444

Manat Kaur − *Structural Biology Department, Stanford University, Stanford, California 94305, United States*

Kensuke Tono − *RIKEN SPring-8 Center, Sayo, Hyogo 679-5148, Japan; Japan Synchrotron Radiation Research Institute, Sayo, Hyogo 679-5198, Japan*

David Adrian Saez − *Departamento de Físico Química, Facultad de Ciencias Químicas, Universidad de Concepción, Concepción 4030000, Chile; Departamento de Farmacia, Facultad de Farmacia, Universidad de Concepción, Concepción 00000, Chile*

Samuel Deutsch − *U.S. Department of Energy Joint Genome Institute, Lawrence Berkeley National Laboratory, Walnut Creek, California 94720, United States*

Yasuo Yoshikuni − *U.S. Department of Energy Joint Genome Institute, Lawrence Berkeley National Laboratory, Walnut Creek, California 94720, United States;* orcid.org/0000-0002-8372-640X

Helmut Grubmüller − *Department of Theoretical and Computational Biophysics, Max Planck Institute for Multidisciplinary Sciences, 37077 Göttingen, Germany;* orcid.org/0000-0002-3270-3144

Complete contact information is available at: https://pubs.acs.org/10.1021/acscentsci.2c00057

Author Contributions

▼H.D., Y.R., G.M.S., B.V., K.S., and A.G. contributed equally.

Notes

The authors declare no competing financial interest.

■ ACKNOWLEDGMENTS

The authors acknowledge Takanori Nakane from the University of Tokyo for his help with calibration of XFEL data from SACLA, RIKEN, Japan. We thank Eriko Nango, Rie Tanaka, and the RIKEN SPring-8 Center for their help with data collection at SACLA, RIKEN, Japan. H.D. acknowledges support from NSF Science and Technology Center grant NSF-1231306 (Biology with X-ray Lasers, BioXFEL). This publication has been produced benefiting from the 2232 International Fellowship for Outstanding Researchers Program and the 1001 Scientific and Technological Research Projects Funding Program of the Scientific and Technological Research Council of Turkey (TÜBİTAK) (Project Nos. 118C270 and 120Z520). However, the entire responsibility of the publication belongs to the authors of the publication. The financial support received from TÜBİTAK does not mean that the content of the publication is approved in a scientific sense by TÜBİTAK. The XFEL experiments were performed at BL3 of SACLA with the approval of the Japan Synchrotron Radiation Research Institute (JASRI) (Proposal No. 2017A8055). The authors thank the beamline staff of the Structural Molecular Biology Group, SSRL, SLAC, and GM/CA CAT, Advance Photon Source, ANL, for assistance with data collection. Y.R., R.G.S., M.S.H., and B.H. were supported by the U.S. Department of Energy, Office of Science, Office of Basic Energy Sciences under Contract No.

DE-AC02-76SF00515. T.J.E. and G.M.S. received support from the Max Planck Society, the European Research Council (ERC 637675 "SYBORG"), and the U.S. Department of Energy Joint Genome Institute, a DOE Office of Science User Facility, under Contract No. DE-AC02-05CH11231. D.A.S., A.G., H.G., and E.V.-M. thank the Max-Planck Society for funding as a Max-Planck-Partner group and CONICYT PCI MPG190003. A.G. acknowledges CONICYT Doctorado Nacional grant 21190262. D.A.S. thanks the Fondo Nacional de Desarrollo Científico y Tecnológico (Fondecyt) for his postdoctoral fellowship No. 3190579. H.D., Y.R., and S.W. are supported by the DOE Office of Science, Biological Environmental Research, and the National Institutes of Health, NIGMS. C.G. and S.W. were supported by the National Science Foundation, Major Research Instrument grant. H.D. and S.W. were partially supported by the Stanford PRECOURT Institute. Gregory M. Stewart of SLAC and Moe Wakatsuki are thanked for graphics work. Coordinates of the four ECR structures have been deposited in the Protein Data Bank under accession codes 6NA3 (apo), 6NA4 (Butyryl-CoA/NADPH bound), 6NA5 (NADP$^+$ bound), and 6NA6 (NADPH-bound).

REFERENCES

(1) Schwander, T.; Schada von Borzyskowski, L.; Burgener, S.; Cortina, N. S.; Erb, T. J. A synthetic pathway for the fixation of carbon dioxide in vitro. *Science (80-.).* **2016**, *354*, 900−904.
(2) Erb, T. J.; et al. Synthesis of C5-dicarboxylic acids from C2-units involving crotonyl-CoA carboxylase/reductase: the ethylmalonyl-CoA pathway. *Proc. Natl. Acad. Sci. U. S. A.* **2007**, *104*, 10631−6.
(3) Schada von Borzyskowski, L.; Rosenthal, R. G.; Erb, T. J. Evolutionary history and biotechnological future of carboxylases. *J. Biotechnol.* **2013**, *168*, 243−251.
(4) Amao, Y. Formate dehydrogenase for CO_2 utilization and its application. *J. of CO2 Utilization* **2018**, *26*, 623−641.
(5) Erb, T. J.; Brecht, V.; Fuchs, G.; Muller, M.; Alber, B. E. Carboxylation mechanism and stereochemistry of crotonyl-CoA carboxylase/reductase, a carboxylating enoyl-thioester reductase. *Proc. Natl. Acad. Sci. U. S. A.* **2009**, *106*, 8871−8876.
(6) Erb, T. J.; Zarzycki, J. Biochemical and synthetic biology approaches to improve photosynthetic CO_2 -fixation. *Curr. Opin. Chem. Biol.* **2016**, *34*, 72−79.
(7) Rosenthal, R. G.; et al. Direct evidence for a covalent ene adduct intermediate in NAD(P)H-dependent enzymes. *Nat. Chem. Biol.* **2014**, *10*, 50−55.
(8) Quade, N.; Huo, L.; Rachid, S.; Heinz, D. W.; Müller, R. Unusual carbon fixation gives rise to diverse polyketide extender units. *Nat. Chem. Biol.* **2012**, *8*, 117−124.
(9) Zhang, L.; et al. Rational Control of Polyketide Extender Units by Structure-Based Engineering of a Crotonyl-CoA Carboxylase/Reductase in Antimycin Biosynthesis. *Angew. Chemie Int. Ed.* **2015**, *54*, 13462−13465.
(10) Stoffel, G. M.; et al. Four amino acids define the CO_2 binding pocket of enoyl-CoA carboxylases/reductases. *Proc. Natl. Acad. Sci. U. S. A.* **2019**, *116*, 13964−9.
(11) Rao, S. T.; Rossmann, M. G. Comparison of super-secondary structures in proteins. *J. Mol. Biol.* **1973**, *76*, 241−56.
(12) Tono, K.; et al. Diverse application platform for hard X-ray diffraction in SACLA (DAPHNIS): application to serial protein crystallography using an X-ray free-electron laser. *J. Synchrotron Radiat.* **2015**, *22*, 532−537.
(13) Chapman, H. N.; et al. Femtosecond X-ray protein nanocrystallography. *Nature* **2011**, *470*, 73−7.
(14) Schlichting, I.; Miao, J. Emerging opportunities in structural biology with X-ray free-electron lasers. *Curr. Opin. Struct. Biol.* **2012**, *22*, 613−26.
(15) Helliwell, J. R. How to solve protein structures with an X-ray laser. *Science* **2013**, *339*, 146−7.
(16) Bernhard, S. A.; MacQuarrie, R. A. Half-site reactivity and the"“" "induced-fit"“" hypothesis. *J. Mol. Biol.* **1973**, *74*, 73−78.
(17) Seydoux, F.; Malhotra, O. P.; Bernhard, S. A.; Stark, G. Half-Site Reactivit. *CRC Crit. Rev. Biochem.* **1974**, *2*, 227−257.
(18) Levitzki, A.; Stallcup, W. B.; Koshland, D. E. Half-of-the-sites reactivity and conformational states of cytidine triphosphate synthetase. *Biochemistry* **1971**, *10*, 3371−3378.
(19) Fersht, A. R.; Mulvey, R. S.; Koch, G. L. E. Ligand binding and enzymic catalysis coupled through subunits in tyrosyl-tRNA synthetase. *Biochemistry* **1975**, *14*, 13−18.
(20) Thompson, J. D.; Higgins, D. G.; Gibson, T. J. CLUSTAL W: improving the sensitivity of progressive multiple sequence alignment through sequence weighting, position-specific gap penalties and weight matrix choice. *Nucleic Acids Res.* **1994**, *22* (22), 4673−4680.
(21) Hill, T. L.; Levitzki, A. Subunit neighbor interactions in enzyme kinetics: half-of-the-sites reactivity in a dimer. *Proc. Natl. Acad. Sci. U. S. A.* **1980**, *77*, 5741−5745.
(22) Levitzki, A.; Koshland, D. E. The Role of Negative Cooperativity and Half-of-the-Sites Reactivity in Enzyme Regulation. *Current Topics in Cellular Regulation* **1976**, *10*, 1−40.
(23) Vivoli, M.; Pang, J.; Harmer, N. J. A half-site multimeric enzyme achieves its cooperativity without conformational changes. *Sci. Rep.* **2017**, *7*, 16529.
(24) Danenberg, K. D.; Danenberg, P. V. Evidence for a sequential interaction of the subunits of thymidylate synthetase. *J. Biol. Chem.* **1979**, *254*, 4345.
(25) Anderson, A. C.; O'Neil, R. H.; DeLano, W. L.; Stroud, R. M. The Structural Mechanism for Half-the-Sites Reactivity in an Enzyme, Thymidylate Synthase, Involves a Relay of Changes between Subunits. *Biochemistry* **1999**, *38*, 13829−13836.
(26) Finer-Moore, J. S.; Lee, T. T.; Stroud, R. M. A Single Mutation Traps a Half-Sites Reactive Enzyme in Midstream, Explaining Asymmetry in Hydride Transfer. *Biochemistry* **2018**, *57*, 2786−2795.
(27) Hammes, G. G.; Benkovic, S. J.; Hammes-Schiffer, S. Flexibility, Diversity, and Cooperativity: Pillars of Enzyme Catalysis. *Biochemistry* **2011**, *50*, 10422−10430.
(28) Peter, D. M. Doctoral Thesis. ETH Zurich: 2016.

NOTE ADDED AFTER ASAP PUBLICATION

This paper was published on April 25, 2022, with an incorrect bond pictured in the Abstract graphic. The corrected version was reposted on May 4, 2022.

https://doi.org/10.1021/acscentsci.2c00057
ACS Cent. Sci. 2022, 8, 1091−1101